Temporal Variability of Land–Atmosphere Coupling and Its Implications for Drought over the Southeast United States

JOSHUA K. ROUNDY

Department of Civil and Environmental Engineering, Princeton University, Princeton, New Jersey

CRAIG R. FERGUSON

Department of Hydrology and Water Resources Engineering, Institute of Industrial Science, University of Tokyo, Tokyo, Japan

ERIC F. WOOD

Department of Civil and Environmental Engineering, Princeton University, Princeton, New Jersey

(Manuscript received 19 June 2012, in final form 25 September 2012)

ABSTRACT

Droughts represent a significant source of social and economic damage in the southeast United States. Having sufficient warning of these extreme events enables managers to prepare for and potentially mitigate the severity of their impacts. A seasonal hydrologic forecast system can provide such warning, but current forecast skill is low during the convective season when precipitation is affected by regionally varying land surface heat flux contributions. Previous studies have classified regions into coupling regimes based on the tendency of surface soil moisture anomalies to trigger convective rainfall. Until now, these classifications have been aimed at assessing the long-term dominant feedback signal. Sufficient focus has not been placed on the temporal variability that underlies this signal. To better understand this aspect of coupling, a new classification methodology suitable at daily time scales is developed. The methodology is based on the joint probability space of surface soil moisture, convective triggering potential, and the low-level humidity index. The methodology is demonstrated over the U.S. Southeast using satellite remote sensing, reanalysis, and hydrological model data. The results show strong persistence in coupling events that is linked to the land surface state. A coupling-based drought index shows good agreement with the temporal and spatial variability of drought and highlights the role of coupling in drought recovery. The implications of the findings for drought and forecasting are discussed.

1. Introduction

In many parts of the world, extreme hydrologic events in the form of floods and droughts are a significant source of social and economic damage. In the United States, the average annual damage due to drought alone is $6–8 billion (Wilhite 2000). The U.S. Southeast is one area that is particularly sensitive to droughts owing to an increasing population and crop production that adds stress to the limited water supply (Seager et al. 2009). The social and economic severity of drought can be reduced through advanced planning given sufficient warning of the event. There have been many studies on developing seasonal hydrologic forecast systems (e.g., Luo et al. 2007); however, most of the skill of a hydrologic forecast system depends on the predictability of the precipitation. The ability to predict precipitation at seasonal time scales requires the ability to estimate the future atmospheric state. The premise of predictability of the atmosphere in the extratropics comes from the slowly varying ocean boundaries that play a role in circulation patterns (i.e., teleconnections), which are usually strongest in the cold season (Palmer and Anderson 1994). In the U.S. Southeast there is some skill in predicting the precipitation due to teleconnections during the wintertime; however, during the summer, when the land conditions are usually the driest and the potential for the development of extreme drought is the highest, the skill is nonexistent (Lavers et al. 2009; Seager et al. 2009).

Corresponding author address: Joshua K. Roundy, Department of Civil and Environmental Engineering, Princeton University, Engineering Quad, Room E2009A P, Princeton, NJ 08544.
E-mail: jroundy@princeton.edu

DOI: 10.1175/JHM-D-12-090.1

Even though the warm season teleconnections are weak and provide no means of predictability, there is still a potential of predictability via soil moisture–precipitation feedbacks (Koster et al. 2004, 2010, 2011). The land–atmosphere interaction (hereafter coupling) impacts the diurnal precipitation cycle through the surface heat and moisture fluxes, which impact the growth and attributes of the atmospheric boundary layer. Modeling studies have shown that soil moisture conditions contributed to drought intensification in the case of the 1988 Great Plains drought (Atlas et al. 1993; Sud et al. 2003). Likewise, Trenberth and Guillemot (1996) argue that soil moisture played a role in perpetuating the drought of 1988 but also played a role in perpetuating the wet conditions in 1993 over the Mississippi River basin. Although the above studies demonstrated a connection between soil moisture and extreme hydrologic events, the precise impact of coupling on warm season precipitation remains unknown, as does the gain in hydrologic forecast skill that incorporating such a mechanism would yield.

There have been numerous modeling studies aimed at understanding the true nature and realism of coupling (Guo et al. 2006; Koster et al. 2006; Dirmeyer et al. 2006; Betts 2009; Santanello et al. 2011). Because of the complex interactions between land and atmosphere and a lack of observations, most studies use numerical models to assess coupling; however, there are many assumptions embedded in the components that describe the interactions between the land and atmosphere that lead to intrinsic model assumptions. Therefore, results about the land–atmosphere interactions are inherently model specific, and their implications for different domains, models, and the real world are unclear. Furthermore, these studies usually focus on a particular event or a long-term-average response in assessing coupling, which leaves much to be understood about the finer temporal scales (e.g., interdaily) of land–atmosphere interactions.

Recently, there have been observational based studies to classify land–atmosphere coupling using satellite remote sensing (Ferguson and Wood 2011; Taylor et al. 2012). The classification scheme in the Ferguson and Wood (2011) study used the convective triggering potential (CTP) and the low-level humidity index (HI), as recommended in the earlier work of Findell and Eltahir (2003a,b). Findell and Eltahir (2003a,b) showed that convective triggering of precipitation was more likely to occur in different subspaces of the CTP–HI space depending on the antecedent soil moisture. However, Ferguson and Wood (2011) showed that the proposed CTP–HI subspaces were too rigid to be globally applicable, which served as the motivation for their generalized probabilistic approach. Specifically, they developed an improved classification scheme that can be applied for different regions and datasets by using distributions of CTP and HI. A limitation of the classification is that it only gives the long-term dominate coupling regime and cannot be used to analyze the temporal variability of land–atmosphere coupling.

In this study, we build off the work done by Findell and Eltahir (2003a) and Ferguson and Wood (2011) to develop a coupling classification scheme that is robust in its ability to be applied for different datasets and different regions but specific enough that it can be used to analyze the temporal variability of coupling. The coupling classification is based on classifying strict areas of coupling in the CTP-HI space for specific datasets and regions on the basis of CTP, HI, and soil moisture observations. Using estimates of the state of the atmosphere (CTP and HI) and the state of the land (soil moisture) from reanalysis, remote sensing, and land surface models, the new coupling classification is applied and evaluated for consistency among datasets and with results from previous studies. Furthermore, the temporal characteristics of the coupled regimes are explored with an emphasis on the role coupling plays in drought. For this reason the U.S. Southeast was chosen as the study area, although the framework developed here could be applied on a global domain.

The remainder of the paper is structured as follows. Section 2 details the datasets that will be used to classify and evaluate coupling. Section 3 provides an overview of the methodology of classification. Section 4 presents the classification results and compares the consistency among datasets. Section 5 gives an assessment of the temporal characteristics of the defined coupling states. Section 6 assesses the connection between the coupling states and drought, followed by section 7, which is the discussion and conclusions.

2. Datasets

The data used in this study serve one of two purposes: as an input to the classification or for evaluation. A list of all datasets with their horizontal and temporal resolution, temporal coverage used in this study, and variables used are given in Table 1. Following the work of Findell and Eltahir (2003a) and Ferguson and Wood (2011), we use two derived atmospheric quantities in the classification scheme, the convective triggering potential (CTP) and humidity index (HI). The development of the CTP and HI are based on the premise that specific atmospheric conditions favor triggering of rainfall over wet (positive feedback) and dry (negative feedback) land surface states. The CTP was derived to diagnose the crucial layer of the atmosphere in terms of boundary

TABLE 1. Description of datasets used in this study. Asterisks indicate variables used for classification of coupling; all others are used for evaluation only. SSO indicates sun synchronous orbit.

Product	Horizontal resolution	Temporal resolution	Temporal coverage	Variables	Reference
MERRA	0.5°	3 hourly	1981–2010	CTP,* HI,* SM,* precipitation	Rienecker et al. (2011)
MLAND	0.5°	3 hourly	1981–2010	SM,* precipitation	Reichle et al. (2011)
AIRS	45 km	SSO	2003–09	CTP,* HI*	Susskind et al. (2011)
AMSR-E	0.25°	SSO	2003–09	SM*	Owe et al. (2008)
VIC	0.125°	Daily	1981–2010	SM,* SM2, SM3	Liang et al. (1994)
NLDAS-2	0.125°	Hourly	1981–2010	Precipitation	Xia et al. (2012)
U.S. Drought Monitor	NA	Weekly	2000–10	Drought index	Svoboda et al. (2002)

layer growth, which is approximately 1–3 km above the surface level. The CTP is a measure of stability in this zone and is calculated by integrating the region between the atmospheric profile and the moist adiabatic temperature lapse rate. Therefore, if the atmospheric profile is close to the dry adiabatic lapse rate, then the CTP is large and favors convection over dry soils where there is larger boundary layer growth. If the atmospheric profile is closer to the moist adiabatic lapse rate, then the CTP will be smaller but still positive, which favors convection over wet soils because of the faster growth of the moist static energy in the boundary layer. If there is a temperature inversion in this zone, then the atmosphere is stable and the CTP is negative. In addition to the CTP, the HI helps to further discriminate between different atmospheric conditions. As the name applies, the HI is a measure of the wetness of the atmosphere and is defined by the 50–150 hPa AGL dewpoint depression. Therefore, a lower value of HI indicates a wetter atmospheric state.

Calculating the CTP and HI requires instantaneous profiles of temperature and humidity. In this study we choose to use atmospheric profiles from reanalysis and remote sensing. We use data from the Modern-Era Retrospective Analysis for Research and Applications (MERRA) (Rienecker et al. 2011) and the Atmospheric Infrared Sounder (AIRS) on board the National Aeronautics and Space Administration *Aqua* satellite. The AIRS data product used in this study is the AIRS/Advanced Microwave Scanning Unit (AMSU) Level 2 Support Product (AIRX2SUP) (Susskind et al. 2011) in which the cloud-clearing algorithm used some of the channels of AMSU. The *Aqua* satellite has a sun synchronous orbit with equatorial crossing times of approximately 1330 and 0130 local time (LT) for the ascending and descending nodes, respectively. The early morning, prior to sunrise and the growth of the boundary layer, is the ideal time for the atmospheric observations of CTP and HI; we therefore choose to use the closest estimate from MERRA, which is 0400 LT, and 0130 LT from AIRS. For specific details on the calculation of the CTP and HI, see Ferguson and Wood (2011).

In addition to the above derived atmospheric quantities, surface soil moisture (SM) is also used in our coupling classification. The SM estimates are taken from MERRA, MERRA-Land (MLAND), Advanced Microwave Scanning Radiometer for Earth Observing System (EOS) (AMSR-E; also on board the *Aqua* satellite), and the Variable Infiltration Capacity (VIC) (Liang et al. 1994) hydrological model. MERRA is coupled to the catchment model (Ducharne et al. 2000; Koster et al. 2000) from which the surface SM is representative of the uppermost 0–2-cm layer. MLAND is an offline simulation of the MERRA land model that uses the forcing from the MERRA reanalysis. The main differences between MERRA and MLAND are that the reanalysis precipitation was corrected using the Global Precipitation Climatology Project (GPCP) version 2.1 and the canopy interception parameters were updated (Reichle et al. 2011).The AMSR-E–based SM estimates generated from the Land Parameter Retrieval Model (LPRM; Owe et al. 2008) are also representative of the top 2-cm soil layer. The VIC model provides estimates representative of the uppermost 10-cm layer of SM. VIC was run in water balance mode forced with meteorological observations from the National Land Data Assimilation System version 2.0 (NLDAS-2; Xia et al. 2012). For consistency, all estimates of SM were converted to their annual, grid-scale product-specific percentile values after spatial aggregation. This was done with the goal of normalizing soil saturation across models and spatial grids.

The first dataset that will be used for evaluation is the associated precipitation with each dataset of SM. The precipitation estimates come from MERRA, MLAND (which is gauge-corrected MERRA), and NLDAS-2 forcing (which drives the VIC model). Here we choose to use the NLDAS-2 precipitation to be evaluated with the AMSR-E dataset. In addition we also use SM from the second (SM2, 30 cm) and third (SM3, 60 cm) soil

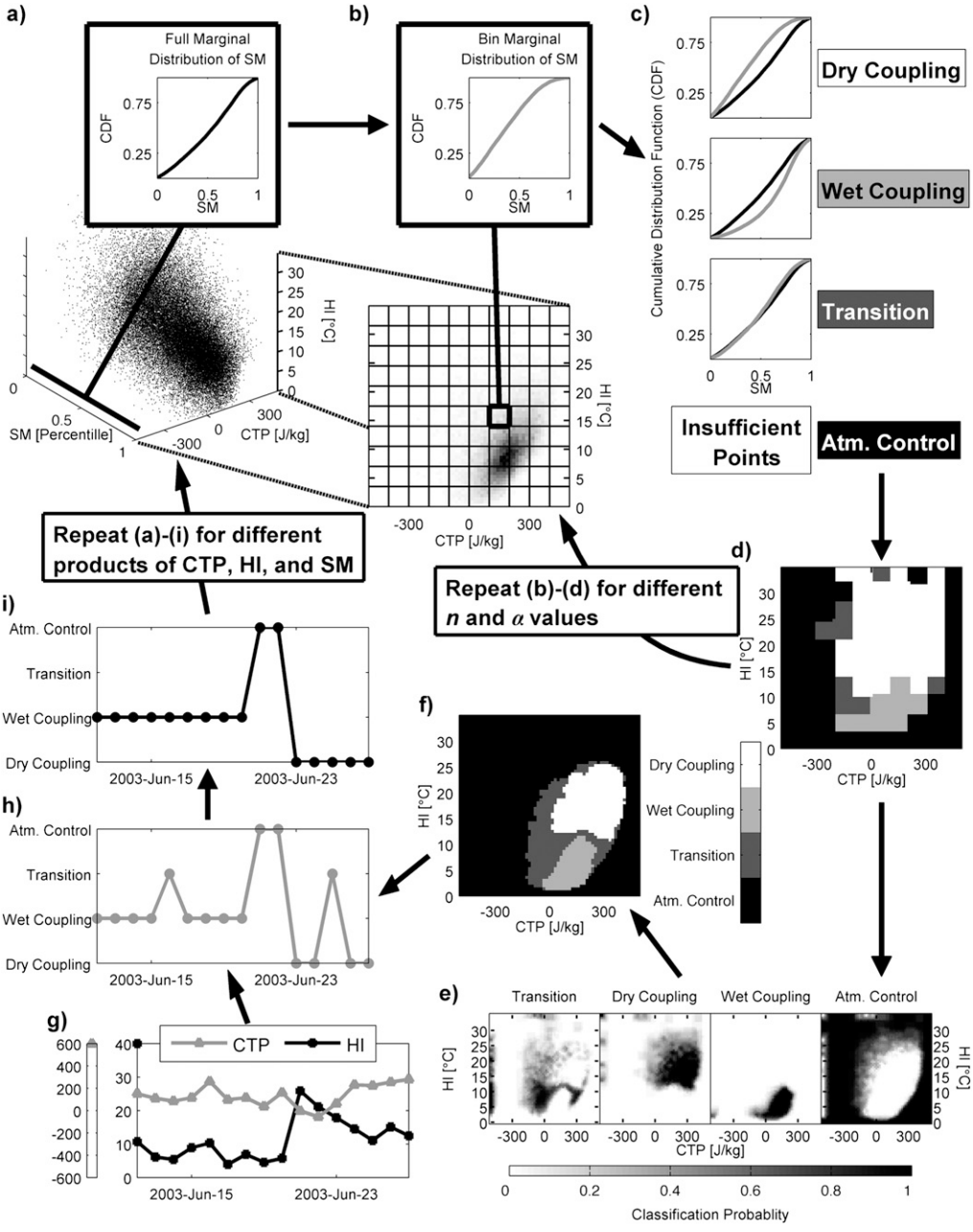

FIG. 1. Flowchart of the methodology. (a) The initial joint CTP–HI–SM space over the U.S. Southeast for the warm season (June–September) from 2003 to 2009. (b) Consider the 2D CTP–HI space with $n \times n$ bins. (c) Classify each bin based on the marginal distributions of SM using a KS test applied with α significance level. (d) Resampling to consistent resolution in the CTP–HI space. (e) Combination of all runs of different n and α values to form probability estimates of classification from which (f) the final classification of the CTP–HI space is derived. Using (f) and (g) the time series of CTP–HI, (h) the time series of coupling is derived. (i) The final coupling time series after a temporal filter and filling in missing values. All subplots use the MERRA CTP–HI and VIC SM. Subplots (a)–(f) consider all 48 grid cells, while subplots (g)–(i) are for a single grid point (34.375°N, 83.125°W).

layers from VIC. To evaluate drought, we use the index from the U.S. Drought Monitor (Svoboda et al. 2002), which classifies drought into to five levels based on a combination of drought metrics: abnormally dry (D0), drought moderate (D1), drought severe (D2), drought extreme (D3), and drought exceptional (D4).

The above data will provide a foundation for classifying and evaluating the temporal variability of land–atmosphere

coupling. These different datasets all vary in spatial resolution (Table 1) but were bin averaged up to a consistent spatial resolution of 1.25° (that of the reduced-resolution MERRA multilevel product), which consists of 48 grid cells in our Southeast (25°–37.5°N, 91.25°–76.25°W) study domain.

3. Classification methodology

The basis for the classification comes from Findell and Eltahir (2003a), which divides up the CTP–HI into strict coupling regimes, that is, atmospherically controlled, transitional, dry soil advantage, and wet soil advantage. The atmospherically controlled regime is the region of the CTP–HI space where the land surface state does not play a role in the triggering of convection. The transitional regime is the area between the dry and wet soil advantage regions. The dry and wet soil advantage regions are areas where the land surface state plays a role in the triggering of precipitation. Specifically, wet soil advantage occurs when the atmospheric state is closer to the wet adiabatic rate, and convection is triggered by a strong increase in the moist static energy from the land surface. In contrast, dry soil advantage occurs when the atmosphere is drier (higher HI) and the temperature profile is close to the dry adiabatic lapse rate (large CTP), which favors convection over areas of large boundary layer growth due to high sensible heat fluxes at the surface.

The Findell and Eltahir (2003a) classification is based on the states of both the land and the atmosphere that are likely to produce convective precipitation. Though the Findell and Eltahir classification captures the precipitation or exchange of water from the atmosphere to the land, it does not consider the exchange of water from the land to the atmosphere. The evaporative demand in the atmosphere between the dry soil advantage and wet soil advantage regime is different because of the larger (drier) values of HI. Therefore, in the absence of convective precipitation, the dry and wet soil advantage regime would lead to persistence of the land surface states. This indicates that evaporation plays a crucial role in the coupling of the land and the atmosphere (Betts 2004). To better capture the drying and wetting of the land surface in our classification methodology, we use soil moisture to classify the CTP-HI space into four coupling regimes similar to the regimes presented by Findell and Eltahir (2003a): atmospherically controlled, transition, dry coupling, and wet coupling. Though the four classifications have similar naming conventions to those of Findell and Eltahir (2003a), we purposely dropped the word "advantage" and added the word "coupling" because our method is based on SM characteristics in the CTP-HI space and is therefore influenced by both precipitation and evaporation. The basis for our methodology is to find areas of the CTP–HI space that are either predominately dry or wet. To do this, we use the concept of SM anomaly applied to the joint CTP–HI–SM space by using the Kolmogorov–Smirnov (KS) two-sample statistical test between a subspace marginal distribution and the full distribution of soil moisture. Once the CTP–HI space is classified, it is then used to create a time series of coupling types, given estimates of CTP–HI. A flowchart of this methodology is given in Fig. 1 and will be discussed below in detail.

The classification starts by considering a joint probability space of CTP–HI and SM at a daily time step for a chosen spatial region over a given time period. For this study, we consider four different combinations of CTP–HI and SM for classifications that will be denoted as CTP-HI dataset–SM dataset. The data pairs include MERRA–MERRA, MERRA–MLAND, MERRA–VIC, and AIRS–AMSR-E. All datasets use the same spatial region, that is, the joint probability space is made up of all 48 land grid points in the U.S. Southeast and the same temporal season, June–September. However, owing to data availability, two study periods are adopted: from 1981 to 2010 for classifications using MERRA CTP–HI and from 2003 to 2009 for those using AIRS CTP–HI. An example of the joint probability space is represented in Fig. 1a, which also illustrates the full marginal distribution of SM illustrated as a cumulative distribution function (CDF). For all subplots of Fig. 1, the MERRA-VIC combination was used with the notable exception that it only considers the 2003–09 time periods for these plots only. This was done in order to assess the impact of a smaller sample on the classification of the CTP–HI space.

The CTP–HI–SM joint probability space is then reduced to the 2D CTP–HI space with $(n \times n)$ bins, where each bin consists of a marginal distribution of soil moisture. To do this, we only consider the humidity index from 0° to 35°C and convective triggering potential from -500 to 500 J kg^{-1}, which is illustrated in Fig. 1b for $n = 10$. Next, each bin is classified by applying the KS test between the bin marginal distribution and the full marginal distribution at a given significance level (α). Based on the results from this test, the bin is then classified into one of four regimes, as illustrated in Fig. 1c. If the KS test indicates that the bin marginal distribution is drier (wetter), then it is classified as dry (wet) coupling. When there is no significant difference between the two distributions, we consider this transition as nearer to climatology because it is neither wet nor dry. We consider a sample size of 20 or less as insufficient to populate a distribution. In such cases, we classify the bin

as atmospherically controlled. Our rationale is based on the idea that coupling is a reoccurring process and the absence of data suggests an inherent randomness.

One limitation to classifying the CTP–HI space in the manner described above (Fig. 1) is that it greatly depends on n and α. To overcome this issue we took an ensemble approach. In doing so, we are able to quantify the uncertainty of the classification due to n and α. Specifically, we used 26 different values of n ranging from $n = 10$ to $n = 35$ and five different significance levels, 95%, 96%, 97%, 98%, and 99%, which gives a total of 130 ensemble members. Because of the different bin size for each ensemble member, each run was regridded to a consistent grid size ($n = 65$). This is illustrated in Fig. 1d, which is the regridding of the $n = 10$ classification to the $n = 65$ bin space. All ensembles of n and α are then used to form a probability estimate of coupling for each regime, at each bin (in $n = 65$ space), as illustrated in Fig. 1e. A classification for each fine-resolution bin ($n = 65$) is determined by the uncertainty estimates for each classification. All bins with a probability of 0.6 or greater for a given regime are classified as that regime. If no regime has a probability of 0.6 or higher, then the bin is classified as transitional. Last, some smoothing of classified space was performed to create contiguous areas in the CTP–HI space, as shown in Fig. 1f. This is the final classification of the CTP–HI space.

The classified CTP–HI space is then used to create a time series of coupling for each spatial grid cell in our U.S. Southeast study domain, illustrated in Fig. 1h for one grid cell (34.375°N, 83.125°W), based on the time series of CTP–HI given in Fig. 1g and the final classification of the CTP–HI space (Fig. 1f). Owing to the inherit nature of the discrete classification, it can give classification jumps at or near the boundaries. This is seen in the initial classification time series (Fig. 1h), which shows three changes in classification, two of which are attributed to boundary conditions. In both cases, the running classification deviated into transitional state for one day and returned to the previous classification on the next. Similarly, there is the potential for atmospherically controlled events to temporarily deviate into other classifications. To overcome these limitations, we apply a two-pass temporal filter. On the first pass, days with coupling (dry, wet, or transition) that are temporally isolated are reclassified as atmospherically controlled. On the second pass, if a multiday coupling event is interrupted at any point in time by an isolated day of another classification, the day is reclassified to match that of the inclusive coupling event. Furthermore, sampling characteristics of remote sensing products preclude continuous long-term coverage. We therefore chose to fill any missing values of CTP–HI in AIRS with the coupling classification from MERRA–VIC. MERRA–VIC was chosen as the SM estimates come from an observationally driven land surface model, which should be a better representation of observed soil moisture. After the temporal filter and filling in of missing values, we arrive at the final classification to be used throughout this analysis (Fig. 1i). The process is the same for each of the different product combinations of CTP, HI, and SM.

4. Classification results

Statistical results from the classification are presented in Figs. 2a,b showing the regime frequency and persistence probabilities. In terms of the raw frequency, all datasets show more wet than dry coupling. Likewise, wet coupling shows a higher persistence probability than dry coupling for all datasets. This suggests that wet coupling is the dominant regime for the Southeast, which is consistent with the long-term wet coupling signal reported by Ferguson and Wood (2011) for 2002–09. In general, the raw persistent probabilities are high for both dry and wet coupling, suggesting that there is temporal structure to these events.

The temporal filter had the largest impact on the atmospherically controlled regime, which showed a substantial increase in both frequency and persistence. In general, the other regimes show a decrease in frequency and an increase in persistence. This suggests that there were more events reclassified due to temporal isolation than those reclassified due to event interruption. The notable exception is the wet coupling frequency for the AIRS–AMSR-E, which showed a small increase. This increase is most likely due to the filling in of missing days from AIRS, which made up 18% of days during the classification period. Of these days, the filling in from MERRA–VIC showed the highest frequency of wet coupling. The combined effect of filling in and the temporal filter made the persistent probabilities of the AIRS–AMSR-E more consistent with the other datasets.

The classification of the CTP–HI space, seen in Fig. 2c, shows distinct areas of wet and dry coupling for all datasets. Although the methodology is unable to yield all dry or all wet classifications, it could yield all transition if there were no spatial patterns of soil moisture. This indicates that MERRA–VIC, which has the lowest frequency of transition, has the strongest spatial patterns in the CTP–HI space. Likewise, the AIRS–AMSR-E, which has the highest frequency of transition, has the weakest spatial patterns. One reason for the weak signal from the AIRS–AMSR-E could be due to the sample size of the SM distributions used in the classification. Even though days with missing values of AIRS are filled in, missing values from AMSR-E, which makes up 25% of

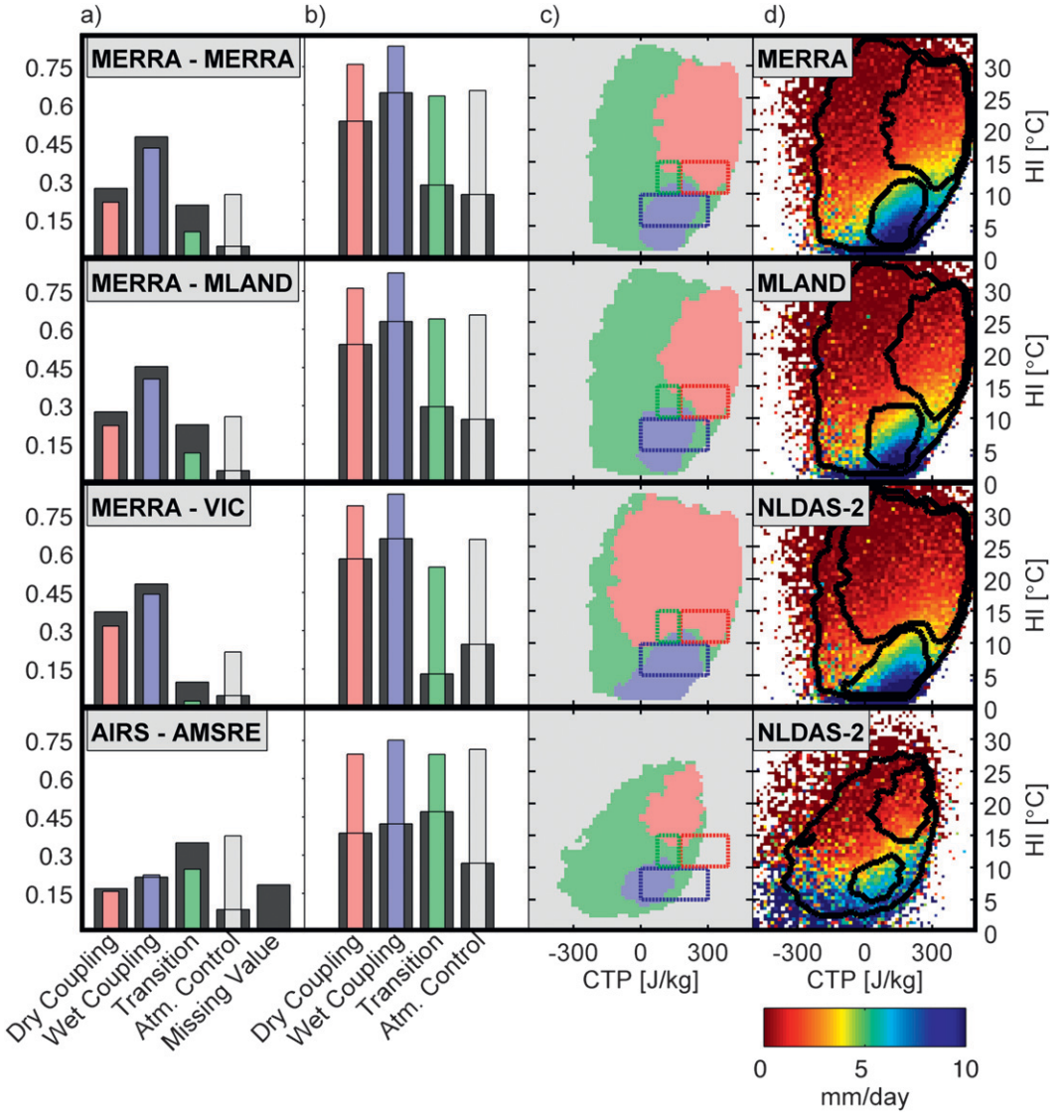

FIG. 2. (a) Normalized frequency (days) and (b) persistence probability of each coupling regime for the warm season in the Southeast before (wide bars) and after (narrow bars) temporal smoothing and filling in missing values (AIRS–AMSR-E only). The data source of CTP and HI is followed by the data source of SM, as in MERRA (CTP, HI) – MERRA (SM). (c) Wet coupling, dry coupling, transition, and atmospherically controlled coupling regime subspaces within the total CTP–HI space with the classification scheme of Findell and Eltahir (2003a) overlaid. (d) Mean daily precipitation (source given in top left corner) in the CTP–HI space overlaid by the classification scheme of this study.

days during the classification period, will reduce the sample size and inherently weaken the signal. The extent to which sample size plays a role in the classification methodology can be assessed by comparing the classification of CTP–HI space for MERRA–VIC from 2003 to 2009 (Fig. 1f) and 1981 to 2010 (Fig. 2c). The shorter time period shows smaller areas, particularly for the dry coupling, but consistent shapes in the CTP–HI classification. This indicates that a reduced sample size weakens the spatial extents in the CTP–HI space, but the general patterns are robust.

The classifications of the CTP–HI space developed in this study for the MERRA datasets show more consistency with the classification from Findell and Eltahir (2003a) than the AIRS dataset (Fig. 2c). The AIRS dataset shows more skew along the CTP axes as compared with the MERRA dataset. This is consistent with the results of Ferguson and Wood (2011), which showed that using the fixed-value coupling classification scheme of Findell and Eltahir (2003a) is not applicable globally. In contrast, the MERRA datasets show similar

structuring of the three coupling regimes to Findell and Eltahir, although the CTP–HI extent is much different. The difference in extent may be partly explained by considering that Findell and Eltahir based their classification on days characterized by the triggering of afternoon convective precipitation. In comparison, the method developed here considers all days. This would suggest that the Findell and Eltahir (2003a) classification is a subset of the classification developed in this study. This idea is further analyzed by comparing the daily average precipitation shown in Fig. 2d with the classifications from this study.

For the MERRA datasets, it can be seen that the dry soil advantage classified by Findell and Eltahir (2003a) intersects the bottom-right area of the dry coupling classification developed in this study. This intersection area can be seen in Fig. 2d as the wettest area of the dry coupling classification in this study. The extended area of the dry coupling classification would fall in the area classified as atmospherically controlled (too dry for rain) by Findell and Eltahir (2003a). Our results indicate that this area is preferential to dry soil. A similar situation exists for the wet soil advantage (Findell and Eltahir 2003a) and wet coupling (this study) classifications. The intersection of these two classifications is seen for the top portion of the wet coupling regime, which is the driest area in terms of precipitation within in the wet coupling regime. Although it is the driest area within the wet coupling, it is still wetter than the wettest area in the dry coupling regime. The extended area of the wet coupling regime, which shows the wettest area of the regime, would be classified by Findell and Eltahir as atmospherically controlled (rain over wet and dry soils). Our classification indicates that this area is dominantly characterized by wet soils. This suggests that the extended areas classified as dry and wet coupling do not play a role in triggering convective precipitation but are still inherently connected by similar SM characteristics.

5. Temporal evolution of coupling

To further understand the characteristics of the coupling regimes defined in this study, we choose to use the temporally smoothed classification because of its increase in consistency between the datasets and to consider only the wet and dry coupling events. An example of dry and wet events for a particular grid cell from the MERRA–VIC combination is shown in Figs. 3a and 3b, which illustrates the temporal evolution of SM, HI, CTP, and precipitation. The soil moisture (circles) for both wet and dry coupling events have periods of drying and wetting. However, because of the frequency and depth of precipitation, the dry coupling event shows longer drying periods. In terms of humidity index (squares), the dry coupling shows a larger variability in comparison to the wet coupling event. This is due to the large area of the CTP–HI space that is classified as dry coupling (Fig. 2b). Both the HI and CTP (triangles) show low variability from day to day during the event. This suggests that dry and wet coupling events are typified by low variability in the atmosphere and distinct differences in SM caused by precipitation frequency and depth.

To better understand the average behavior of the dry and wet coupling events, we use all events from the 48 grids in the study domain to compute the average evolution of SM, HI, and CTP during an event. This is done by binning all events by their initial value of SM, HI, or CTP and then taking an average of all events within the bin for each day of the event. For example, a day 1 average for the 90th–100th percentile bin of SM for wet coupling would be computed by taking all wet coupling events with an initial SM between the 90th and 100th percentile and then taking the average of all day 1 for those events. This is repeated for all days with at least 10 events. In addition, the CTP values that are less than -500 J kg^{-1} are ignored when computing the average. This only occurred less than 1% of the time. These results are plotted in the first three rows of Fig. 4.

Considering the evolution of the convective triggering potential and humidity index, it can be seen that both variables tend to a distinct equilibrium for dry and wet events and show very little persistence of the initial condition. One key difference between the CTP and HI and the SM is the separation of dry and wet events by the initial value. The initial value of HI shows a strong separation between dry and wet coupling. The CTP shows less separation between events than HI but more than SM. The SM shows no separation as there are dry coupling events that start really wet, and wet coupling event that start really dry. This indicates that the initial SM does not determine the coupling event. The determination of the coupling event is mostly controlled by the HI. This behavior is directly linked to the classification of the CTP–HI space, shown in Fig. 2, by the general separation of the dry and wet areas in HI dimension.

Though the HI plays the primary role in determination of the coupling event, the SM plays a role in persistence of the event. This is shown in the bottom row of Fig. 4, which gives the average event duration for the initial soil moisture. For dry coupling events, the average duration decreases as the initial SM increases. In contrast, the average duration increases as SM increases for wet coupling events. This behavior demonstrates that the initial SM plays a role in the persistence of the event and is observed for all datasets, although the AIRS–AMSR-E shows a weaker relationship for drier soils.

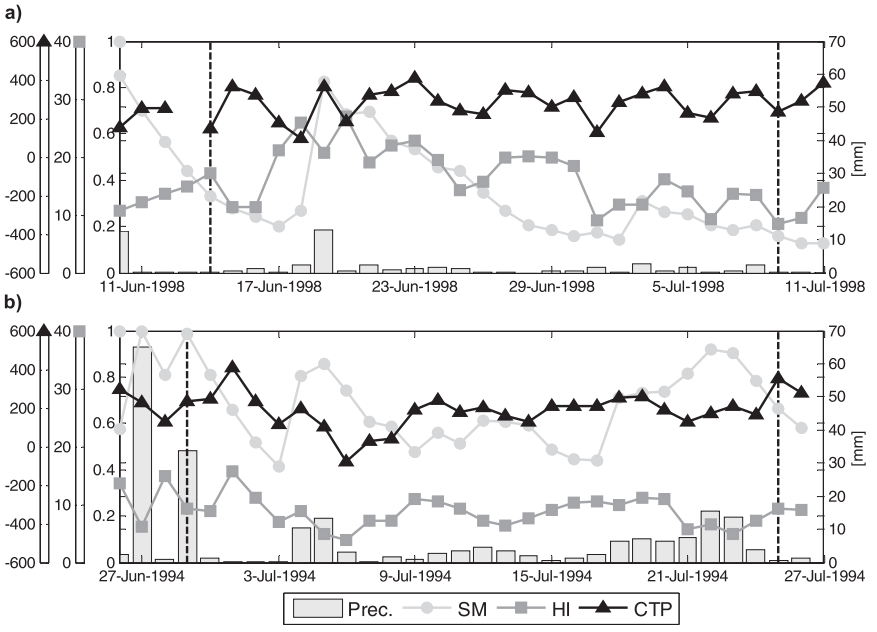

FIG. 3. Examples of (a) dry and (b) wet coupling events for an arbitrary grid cell (34.375°N, 81.875°W) in the Southeast, classified using MERRA-VIC and using the NLDAS-2 daily precipitation. Vertical dotted lines indicate the start and end of each event. Values of CTP < -500 J kg^{-1} are removed for clarity.

The largest difference in behavior among the classifications seen in Fig. 4 is for SM. Of the three MERRA datasets the MERRA–VIC shows the closest relationship to the AIRS–AMSR-E. Both datasets show a tendency toward an equilibrium for both dry and wet coupling events. This is seen for dry coupling events by an increase in SM for the driest initial conditions. Likewise, the wet coupling events show a decrease in SM for the wettest initial conditions. In addition, the rate at which the wet equilibrium is reached is much faster than the dry. This makes sense as the process that drives soil wetting (precipitation) is a fast process while that of drying (evaporation) is inherently slower. In comparison, the MERRA–MERRA and the MERRA–LAND show consistent drying (dry coupling) and wetting (wet coupling) for all initial conditions. Furthermore, they also show a stronger persistence of initial conditions. The difference between the MERRA classifications suggests that there is a dampening of the atmospheric signal in the MERRA–MERRA and MERRA–MLAND classifications. Such behavior would be expected for deeper soil layers. This is illustrated in Fig. 5, which shows the same plot as Fig. 4 for the three soil layers of the VIC model using the MERRA–VIC classification to define the coupling events. This shows that the deeper the layer, the less pronounced the equilibrium becomes. It can also be seen that the deepest soil layer from VIC compares more closely with top layers from MERRA and MLAND.

6. Coupling events and drought

The consistent drying (dry coupling events) and wetting (wet coupling events) seen in Fig. 5c for the deep VIC soil layers suggests a connection between the coupling events and drought. This indicates that the dry coupling events are associated with continuation and intensification of drought (drying of deep soil layers), while wet coupling events are associated with drought recovery (wetting of deep soil layers). Therefore, multiple events during a time period would be indicative of hydrologic extremes such as drought and flood. On this basis, we define the coupling drought index (CDI) by considering the number of days in a dry or wet coupling event over a period of time:

$$\mathrm{CDI} \equiv \frac{N_d - N_w}{N_t},$$

where N_d is the number of dry coupling days, N_w is the number of wet coupling days, and N_t the total number of days during a time period. The CDI has a minimum value of -1, indicating every day during the period is a wet coupling event (drought recovery). It also has a maximum value of $+1$, indicating every day is a dry coupling event (intensification and persistence of drought). If the number of wet coupling days equals the number of dry coupling days, it is assumed that there is no net effect toward or away from drought. By design, the CDI captures

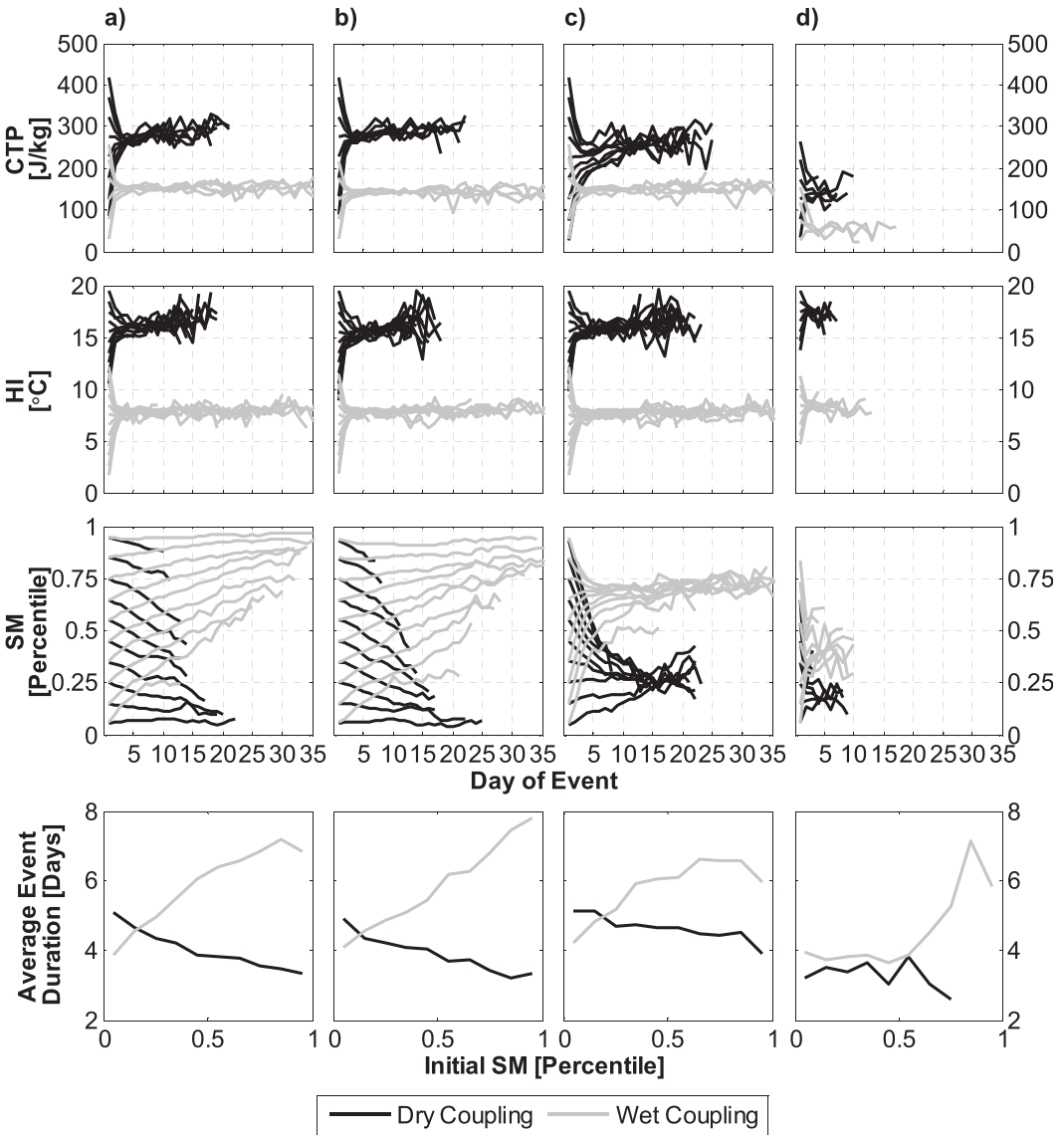

FIG. 4. The average evolution of SM, HI, and CTP (top three rows from top to bottom) during the coupling event separated by initial values and average event duration (bottom row) based on initial SM for (a) MERRA–MERRA, (b) MERRA–MLAND, (c) MERRA–VIC, and (d) AIRS–AMSR-E for the Southeast warm season.

only the response to drought due to coupling, which can be thought of as the impact of both precipitation and evaporation on drought. The transition of atmospherically controlled events act to drive the CDI toward zero, independent of their actual contribution to recovery or intensification of drought.

The spatial averaged seasonality of the CDI for all the datasets (Fig. 6a) is shown along with the conventional drought monitor (Fig. 6b). MERRA–VIC has a similar seasonality to AIRS–AMSR-E, while the MERRA–MERRA is very similar to the MERRA–MLAND. In general, all datasets show the same seasonality of CDI with a maximum (drought) in May and minimum (recovery) in August–September. In comparison, the U.S. Drought Monitor (Fig. 6b) also shows a peak in D0–D2 droughts in May and a peak in D2–D4 in August. This indicates that, as the summer progresses, the predominant coupling regime changes from dry to wet, during which the potential for extreme drought increases. This behavior is consistent as periods typified by drought recovery have the potential to turn into extreme droughts if the recovery mechanism is absent. This underscores the importance of land–atmosphere interactions to drought recovery in the late summer months over the Southeast.

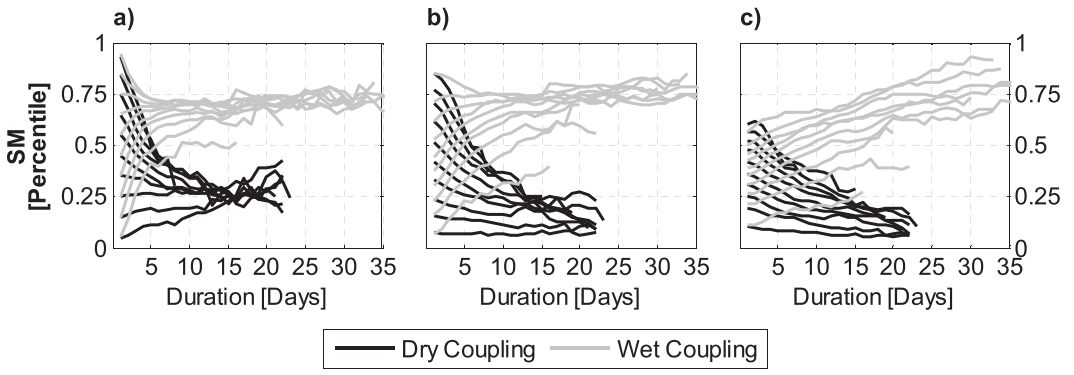

FIG. 5. Average evolution of SM during the coupling event separated by initial values (as in the top row of Fig. 5) based on MERRA–VIC for (a) soil layer 1 (0–0.1 m), (b) 2 (0.1–0.4 m), and (c) 3 (0.4–1.0 m) for the Southeast warm season.

The temporal and spatial variability of drought given by the U.S. Drought Monitor and the CDI are shown in Fig. 7 for June–July for seven consecutive years. The June–July time period was chosen as it is in between the minimum and maximum seasonal CDI and therefore should have a greater temporal variability. The U.S. Drought Monitor shows 2003–05 as years of no drought or drought recovery. These years have a very negative CDI, indicating no drought. The coupling drought index is also consistent with the U.S. Drought Monitor for years generally typified by drought persistence and intensification (2006–09). In particular, the CDI for 2006 shows strong intensification of drought in the Southeast, with exception of the Florida peninsula, which shows recovery. Spatial patterns of intensification and recovery are also consistent for 2007. It is interesting that the CDI for all datasets is the strongest in 2006, while the U.S. Drought Monitor shows a more intense drought in 2007. The difference in the CDI between these two years can be attributed to the initial state of drought at the beginning of June. In 2006 there is little or weak drought initially, while in 2007 the drought was already fairly intense. This suggests that large values of CDI are characteristic of drought development, but drought can persist with smaller positive values. Overall, the CDI for all classifications of coupling are generally consistent with the U.S. Drought Monitor for all years considered, which illustrates the role coupling plays in drought evolution.

7. Discussion and conclusions

This study set out to bridge the gap in understanding the finer temporal scales of land–atmosphere coupling using an observational framework. To do this, we developed a new method to classify the CTP–HI space into four classifications based on distributions of soil moisture. One of our main findings is that the resulting coupling

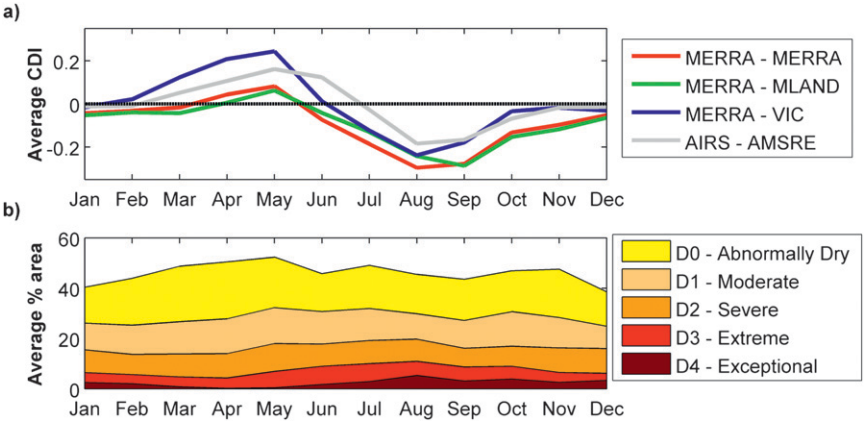

FIG. 6. Seasonality of (a) the coupling drought index (CDI) for all classifications and (b) the average percent area of drought severity from the U.S. Drought Monitor for the Southeast for the period of 2000–10. Owing to data availability, AIRS–AMSR-E is for 2003–09 only.

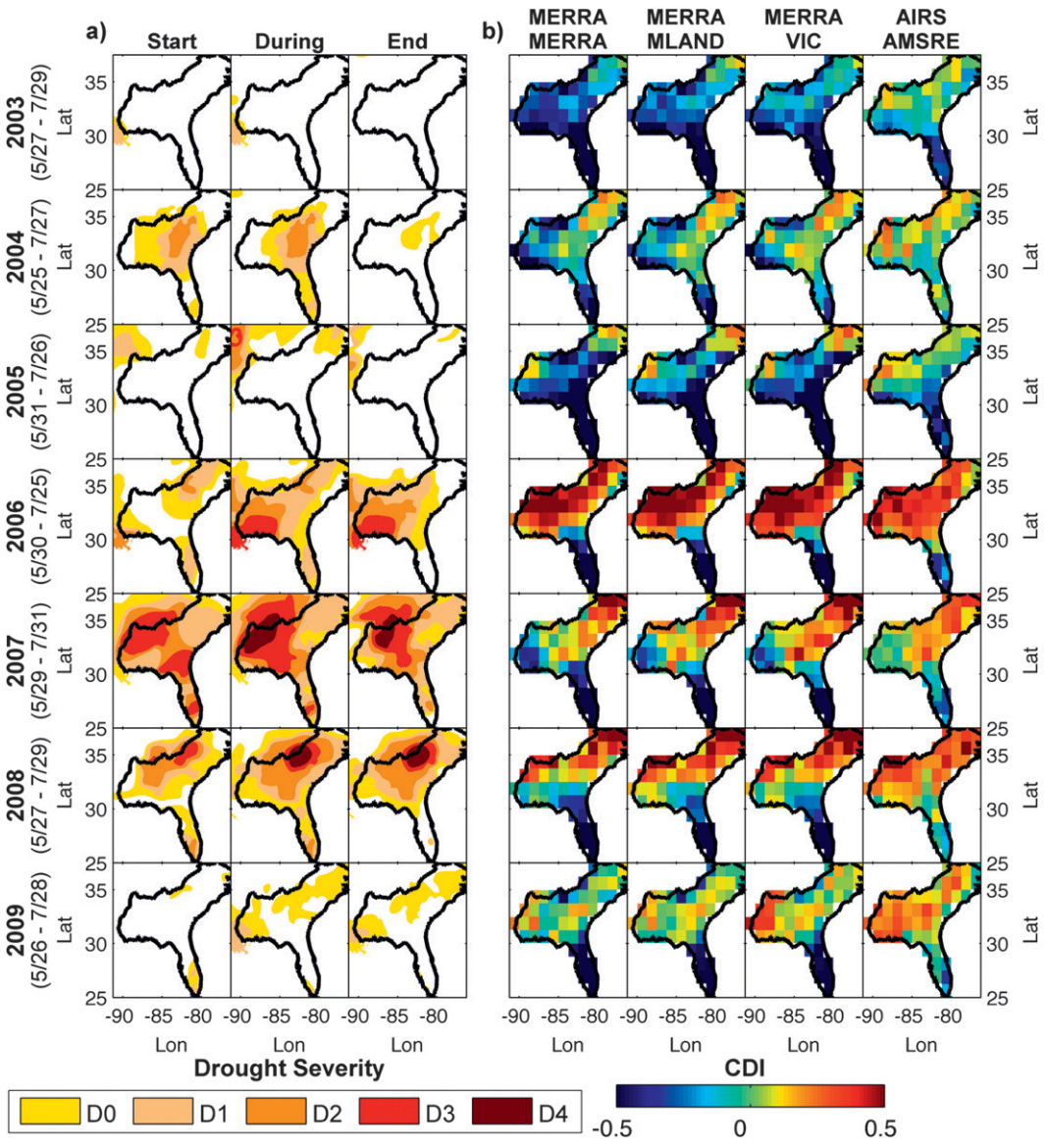

FIG. 7. The spatial and temporal variability of the 2003–09 June–July (a) drought severity for the start, duration, and end of the time period and (b) derived CDI using various input datasets.

classifications demonstrate high temporal persistence, which allowed evaluation of the temporal characteristics of these events. Our classification results confirmed the long-term classification of Ferguson and Wood (2011) for the U.S. Southeast and showed that there is a distinct seasonality of the coupling events. The dry soil and wet soil advantage classifications of Findell and Eltahir (2003a) were shown to be a subset of the dry and wet coupling events defined in this study. The dry and wet coupling events were shown to have different characteristics and opposing implications to the regional hydrologic cycle due to the frequency and depth of precipitation. The tendency of SM during these events was shown to be toward a distinct equilibrium for dry and wet events. It was also shown that the initiation of wet or dry coupling events was mainly controlled by the humidity index and that the soil moisture played a role in the persistence.

The characteristics of the dry and wet events demonstrated in this study are similar to those demonstrated by Rodriguez-Iturbe et al. (1991). In their study, they used a physically based model with components that account for local recycling of precipitation to show that stochastic fluctuations in the precipitation forcing lead to a bimodal (dry and wet) long-term distribution of soil moisture. They also suggest that there is persistent

behavior in one mode, until the forcing is large enough to perturb it from one stable node into the other (Rodriguez-Iturbe et al. 1991). The results presented here suggest that precipitation recycling plays an important role on time scales on the order of days. The link to drought through the derived coupling drought index based on the frequency of days in a dry or wet coupling event demonstrated this importance. Furthermore, the seasonality of the CDI indicated that the late summer months were predominantly wet coupling and therefore important for drought recovery. This is a key finding of our study because it contributes to our understanding of drought dynamics in the Southeast. Though the results presented here only apply to the U.S. Southeast, this framework could be extended to other regions of the United States and globally.

Though the primary application of CDI demonstrated in this study would be for drought monitoring, it could be useful in the prediction of both drought and flood. The ability to predict future coupling would require models that can reproduce the ''true'' nature of the land–atmosphere coupling. The AIRS–AMSR-E sensor datasets, from the NASA *Aqua* satellite, used in this study provide the only observations of coupling at continental to global scales—a capability now lost with the failure of AMSR-E. Other satellite measurements of soil moisture could be used, such as AMSR2 or Soil Moisture and Ocean Salinity (SMOS) [or, in the future, Global Change Observation Mission-Water (GCOM-W1) or Soil Moisture Active Passive (SMAP)]. The simultaneous observations of atmospheric variables from AIRS and soil moisture from AMSR-E provide a unique capability that appears to be permanently lost at this time. Of the other datasets, the MERRA–VIC showed the closest resemblance to AIRS–AMSR-E in terms of the characteristics of event evolution. In particular, the MERRA–MERRA and MERRA–LAND did not show a tendency to a dry or wet equilibrium for soil moisture. In fact, the top-layer SM from MERRA–MERRA and MERRA–MLAND showed similar characteristics to the third layer in the VIC model. This suggests that the top soil layer in MERRA acts more like a deep soil layer in terms of its coupling to the atmosphere. A true attribution of this behavior would require running multiple land models using different forcing and parameters and is outside the scope of this work. However, the framework developed here provides a meaningful way of assessing the land–atmosphere interactions for different land surface models and forcings.

The importance of the land surface model in forecasting was also demonstrated by the finding that the land surface plays a role in the persistence of the events. This demonstrates the importance of initial conditions and the ability of forecast models to persist in either dry or wet events. This leads to the question: do current coupled forecast models, such as the National Centers for Environmental Prediction (NCEP) Climate Forecast System, version 2 (CFSv2), show the same characteristics in the CTP–HI–SM space as demonstrated here? Our preliminary studies (not shown) suggest that the model is unable to persist in dry or wet events but tends to the mean. We speculate that this shortcoming could be part of the reason why there is little skill in seasonal forecasts during the warm season. Furthermore, there is also the potential of developing statistical models for the summer months on the basis of initial conditions, persistent probabilities, and precipitation characteristics observed in this study. These questions are left for future work.

Acknowledgments. J. K. Roundy was supported through NASA Earth and Space Science Fellowship NNX08AU28H (Understanding Hydrologic Sensitivity and Land–Atmosphere Coupling through Space-Based Remote Sensing) and NOAA Grant NA08OAR4320915 (Ensemble Hydrologic Forecasts over the Southeast in Support of the NIDIS Pilot). C. R. Ferguson is supported by the Japan Society for the Promotion of Science Postdoctoral Fellowship for Foreign Researcher P10379.

REFERENCES

Atlas, R., N. Wolfson, and J. Terry, 1993: The effect of SST and soil-moisture anomalies on GLA model simulations of the 1988 U.S. summer drought. *J. Climate,* **6,** 2034–2048.

Betts, A. K., 2004: Understanding hydrometeorology using global models. *Bull. Amer. Meteor. Soc.,* **85,** 1673–1688.

——, 2009: Land–surface–atmosphere coupling in observations and models. *J. Adv. Model. Earth Syst.,* **1,** 18 pp. [Available online at http://james.agu.org/index.php/JAMES/article/view/v1n4.]

Dirmeyer, P. A., R. D. Koster, and Z. Guo, 2006: Do global models properly represent the feedback between land and atmosphere? *J. Hydrometeor.,* **7,** 1177–1198.

Ducharne, A., R. D. Koster, M. J. Suarez, M. Stieglitz, and P. Kumar, 2000: A catchment-based approach to modeling land surface processes in a general circulation model: 2. Parameter estimation and model demonstration. *J. Geophys. Res.,* **105,** 24 823–24 838.

Ferguson, C. R., and E. F. Wood, 2011: Observed land–atmosphere coupling from satellite remote sensing and reanalysis. *J. Hydrometeor.,* **12,** 1221–1254.

Findell, K. L., and E. A. B. Eltahir, 2003a: Atmospheric controls on soil moisture–boundary layer interactions. Part I: Framework development. *J. Hydrometeor.,* **4,** 552–569.

——, and ——, 2003b: Atmospheric controls on soil moisture–boundary layer interactions. Part II: Feedbacks within the continental United States. *J. Hydrometeor.,* **4,** 570–583.

Guo, Z., and Coauthors, 2006: GLACE: The Global Land–Atmosphere Coupling Experiment. Part II: Analysis. *J. Hydrometeor.,* **7,** 611–625.

Koster, R. D., M. J. Suarez, A. Ducharne, M. Stieglitz, and P. Kumar, 2000: A catchment-based approach to modeling land surface processes in a general circulation model: 1. Model structure. *J. Geophys. Res.,* **105,** 24 809–24 822.

——, and Coauthors, 2004: Regions of strong coupling between soil moisture and precipitation. *Science,* **305,** 1138–1140.

——, and Coauthors, 2006: GLACE: The Global Land–Atmosphere Coupling Experiment. Part I: Overview. *J. Hydrometeor.,* **7,** 590–610.

——, and Coauthors, 2010: Contribution of land surface initialization to subseasonal forecast skill: First results from a multimodel experiment. *Geophys. Res. Lett.,* **37,** L02402, doi:10.1029/2009GL041677.

——, and Coauthors, 2011: The second phase of the Global Land–Atmosphere Coupling Experiment: Soil moisture contributions to subseasonal forecast skill. *J. Hydrometeor.,* **12,** 805–822.

Lavers, D., L. F. Luo, and E. F. Wood, 2009: A multiple model assessment of seasonal climate forecast skill for applications. *Geophys. Res. Lett.,* **36,** L23711, doi:10.1029/2009GL041365.

Liang, X., D. P. Lettenmaier, E. F. Wood, and S. J. Burges, 1994: A simple hydrologically based model of land surface water and energy fluxes for general circulation models. *J. Geophys. Res.,* **99,** 14 415–14 428.

Luo, L. F., E. F. Wood, and M. Pan, 2007: Bayesian merging of multiple climate model forecasts for seasonal hydrological predictions. *J. Geophys. Res.,* **112,** D10102, doi:10.1029/2006JD007655.

Owe, M., R. de Jeu, and T. Holmes, 2008: Multisensor historical climatology of satellite-derived global land surface moisture. *J. Geophys. Res.,* **113,** F01002, doi:10.1029/2007JF000769.

Palmer, T. N., and D. L. T. Anderson, 1994: The prospects for seasonal forecasting—A review paper. *Quart. J. Roy. Meteor. Soc.,* **120,** 755–793.

Reichle, R. H., R. D. Koster, G. J. M. De Lannoy, B. A. Forman, Q. Liu, S. P. P. Mahanama, and A. Toure, 2011: Assessment and enhancement of MERRA land surface hydrology estimates. *J. Climate,* **24,** 6322–6338.

Rienecker, M. M., and Coauthors, 2011: MERRA: NASA's Modern-Era Retrospective Analysis for Research and Applications. *J. Climate,* **24,** 3624–3648.

Rodriguez-Iturbe, I., D. Entekhabi, and R. L. Bras, 1991: Nonlinear dynamics of soil moisture at climate scales: 1. Stochastic analysis. *Water Resour. Res.,* **27,** 1899–1906.

Santanello, J. A., C. D. Peters-Lidard, and S. V. Kumar, 2011: Diagnosing the sensitivity of local land–atmosphere coupling via the soil moisture–boundary layer interaction. *J. Hydrometeor.,* **12,** 766–786.

Seager, R., A. Tzanova, and J. Nakamura, 2009: Drought in the southeastern United States: Causes, variability over the last millennium, and the potential for future hydroclimate change. *J. Climate,* **22,** 5021–5045.

Sud, Y. C., D. M. Mocko, K. M. Lau, and R. Atlas, 2003: Simulating the Midwestern U.S. drought of 1988 with a GCM. *J. Climate,* **16,** 3946–3965.

Susskind, J., J. M. Blaisdell, L. Iredell, and F. Keita, 2011: Improved temperature sounding and quality control methodology using AIRS/AMSU data: The AIRS Science Team Version 5 retrieval algorithm. *IEEE Trans. Geosci. Remote Sens.,* **49,** 883–907.

Svoboda, M., and Coauthors, 2002: The drought monitor. *Bull. Amer. Meteor. Soc.,* **83,** 1181–1190.

Taylor, C. M., R. A. M. de Jeu, F. Guichard, P. P. Harris, and W. A. Dorigo, 2012: Afternoon rain more likely over drier soils. *Nature,* **489,** 423–426.

Trenberth, K. E., and C. J. Guillemot, 1996: Physical processes involved in the 1988 drought and 1993 floods in North America. *J. Climate,* **9,** 1288–1298.

Wilhite, D. A., 2000: Drought as a natural hazard: Concepts and definitions. *Drought: A Global Assessment.,* D. A. Wilhite, Ed., Hazards and Disaster Series, Vol. 2, Routledge, 3–18.

Xia, Y., and Coauthors, 2012: Continental-scale water and energy flux analysis and validation for the North American Land Data Assimilation System project phase 2 (NLDAS-2): 1. Intercomparison and application of model products. *J. Geophys. Res.,* **117,** D03109, doi:10.1029/2011JD016048.